https://doi.org/10.5194/egusphere-2026-4351
Preprint. Discussion started: 28 September 2026

Age and basal conditions using a 2.5D ice flow model constrained by radar horizons along the Dome Fuji–EDML flow line, Antarctica

Ailsa Chung[1,2,3], Yéva Jeaumot[1], Frédéric Parrenin[1], Daniel Steinhage[4], and Olaf Eisen[4,5]

[1]Université Grenoble Alpes, CNRS, INRAE, IRD, Grenoble INP, IGE,Grenoble, France
[2]Climate and Environmental Physics, Physics Institute, University of Bern, Bern, Switzerland
[3]Oeschger Centre for Climate Change Research, University of Bern, Bern, Switzerland
[4]Alfred-Wegener-Institut Helmholz-Zentrum für Polar-und Meeresforschung, Bremerhaven, Germany
[5]Fachbereich Geowissenschaften, Universität Bremen, Bremen, Germany

Correspondence: Ailsa Chung (ailsa.chung@unibe.ch)

Abstract.

Ice flow modelling is important for understanding the factors that affect overall ice sheet dynamics. We apply a 2.5D inverse flow tube model to the flow line from Dome Fuji (DF) to the EPICA Dronning Maud Land (EDML) ice core site in East Antarctica. The model is constrained by eight continuous and five discontinuous internal reflecting horizons traced from radar surveys and dated by connecting them to the DF ice core. The flow tube was determined by following the steepest slope of surface elevation from EDML upstream to DF. The aim of this study is to estimate basal melt rates, accumulation rates, particle trajectories, the age of ice and the thinning function along the flow line and compare results to previous modelling and observation work.

We find that basal melting is highest where there are dips in the bedrock, whereas stagnant ice tends to occur on or slightly downstream of bedrock rises. The modelled accumulation rate generally increases with proximity to the coast, agreeing well with previous studies. Modelling particle trajectories gives us an understanding of the deposition location and therefore altitude and temperature, allowing measurements from the deepest and oldest ice in the EDML ice core to be corrected accordingly. Results show that the oldest ice from the EDML ice core may have come from up to 130 km upstream. This is significantly closer to the ice core site than previous estimates. Modelled surface velocity magnitudes around EDML match those found by observations. We also identify one area around 200 km from the DF summit, where the modelled maximum age of ice is > 1 Ma.

1 Introduction

Ice cores are invaluable climate archives that give us a unique look into the past atmospheric gas composition through direct measurements of air bubbles trapped in the ice (Lüthi et al., 2008; Petit and Raynaud, 2020). They also provide local temperature reconstructions based on ice isotopic variations (Grisart et al., 2022), while aerosol and dust content provide insights into atmospheric transport and the climate of source regions (Fischer et al., 2007; Vanderstraeten et al., 2023). In order to retrieve the longest ice core record possible, drilling projects search for potential places where ice is old and layers are well preserved

https://doi.org/10.5194/egusphere-2026-4351
Preprint. Discussion started: 28 September 2026

(Fischer et al., 2013). To that end, the International Partnership in Ice Core Science (IPICS) launched the Oldest Ice challenge to drill an ice core covering the last 1.2 Ma of climate history (Dahl-Jensen, 2018; Wolff et al., 2020). Ice cores provide high resolution information throughout the ice column, but only at a single location.

Radar surveys complement ice cores, as they can cover extended areas, giving us 2D cross-sections of the internal stratigraphy of the ice sheet along a transect (Bingham et al., 2025). The layers seen in radargrams, known as internal reflection horizons (IRHs), can be ancient surfaces of the ice sheet pushed down by the weight of accumulation on top (Eisen et al., 2006). Although the vertical resolution of a radargram is lower than that of an ice core, it is nevertheless possible to attribute ages to IRHs by connecting them to ice core chronologies (Cavitte et al., 2016; Bingham et al., 2025). This effectively extends the ice core age-depth relationship spatially to other areas of the ice sheet. The shape of IRHs can give information on deposition conditions such as accumulation (Waddington et al., 2007) and past ice sheet dynamics such as basal melting (Siegert and Hodgkins, 2000; Jordan et al., 2018) and ice flow divergence (Hindmarsh et al., 2006). The challenge is disentangling how and to what extent each of these processes have contributed to the current shape of the IRHs (Ashmore et al., 2020; Sutter et al., 2021), thereby giving us an understanding of how the ice dynamics have changed over time.

Models of different complexities are often used to assess the contribution of each process in both Greenland and Antarctic ice sheets (e.g. Obase et al., 2023; Gerber et al., 2021; Born and Robinson, 2021). 3D regional or continental scale models are the most complex. They can consider many different parameters and have the advantage of being transient (Sutter et al., 2019; Albrecht et al., 2020a). However, due to their expensive computation, some processes are simplified and resolution is multi-kilometric (Golledge et al., 2015). Characterising conditions such as basal melting is therefore difficult as it is highly dependant on local conditions which may not be well represented. Using observational constraints during the model evolution would be even more computationally heavy, and it is often difficult to match the modelled present day ice sheet coverage to current topography observations (Albrecht et al., 2020a, b), making comparison to radar IRHs even more challenging (Sutter et al., 2021).

Chung et al. (2023) developed a 1D inverse model that used radar IRH constraints to look at the age-depth profile around Dome C, Antarctica. The model also determines where basal melting or a layer of stagnant ice occurs. Stagnant ice in the modelling community is defined as a layer of ice just above the bedrock, where a vertical velocity of zero is inferred. This model has also been applied to Dome Fuji (DF, Wang et al., 2023) and Dome A (Li et al., 2026), showing that the 1D assumption is reasonable in areas with little to no horizontal flow. However, at other locations where ice dynamics are more complex, 1D models are too simplistic. Parrenin et al. (2025) developed a 2.5D model that takes into account horizontal flow divergence by means of a flow tube width, based on earlier work from Parrenin and Hindmarsh (2007). Chung et al. (2025) developed this into an inverse model constrained by radar IRHs and applied it to a flow line from Dome C (DC) to Little Dome C (LDC), to assess the affect of horizontal ice flow on the Beyond EPICA ice core located in that area. Jeaumot et al. (2026, in review) have since improved this 2.5D model by including a more realistic representation of basal conditions. While the benefits of this model relative to the 1D model were limited at Dome C, the 2.5D model would be better suited to a flow line such as that from DF to the EPICA Dronning Maud Land (EDML) ice core where the effect of horizontal flow is significant.

https://doi.org/10.5194/egusphere-2026-4351
Preprint. Discussion started: 28 September 2026

Wesche et al. (2007) used a network of stakes surveyed by GPS measurements to determine the surface strain field in the vicinity of EDML, and thus infer dynamic vertical thinning. However, there are no detailed horizontal flow observations along the divide from DF to EDML. Huybrechts et al. (2007) used a 3D thermomechanical model with Lagrangian backtracing method to determine thinning and the particle trajectories of ice in the EDML ice core. They found that the deepest ice came from almost 200 km upstream and that the thinning function is relatively linear. They highlighted that due to snow being deposited at higher elevation, biases in results could be up to half the magnitude of the temperature signal from δ^{18}O, during the Last Interglacial period. Therefore it is especially important to account for the upstream position of the ice particle deposition when interpreting the climatic signal measured in the ice.

The aim of this study is to assess the age-depth profile, basal conditions and particle trajectories along the flow line from DF to EDML using a 2.5D inverse model constrained by radar IRHs. Comparison with a more complex model (Huybrechts et al., 2007) and surface velocity observations (Wesche et al., 2007) at EDML acts as a validation study. Meanwhile, modelling conditions upstream improves understanding of ice sheet dynamics in the region. We define a 1130 km flow line from EDML to DF by following the surface slope of the ice sheet upstream. We apply the 2.5D inverse model presented in Jeaumot et al. (2026, in review) to the flow line using the eight continuous IRHs from Steinhage et al. (2013) and five deeper, discontinuous IRHs, as constraints. The modelled accumulation rate follows the expected trend of generally increasing with proximity to the coast. Stagnant ice is generally modelled on bedrock peaks or slightly downstream and basal melting occurs elsewhere. Particle trajectories show that the deepest ice in the EDML ice core comes from around 130 km, closer than was found by Huybrechts et al. (2007). Modelled surface velocity magnitudes agree well with observations made by Wesche et al. (2007) near EDML. From the age-depth profile we also identify an area that we label Dome Fuji Saddle (DFS), at around 200 km from DF with ice potentially >1 Ma, which could be of interest for the IPICS Oldest Ice challenge.

2 Method

The mathematical foundation of the model used in this work was first proposed by Parrenin and Hindmarsh (2007) and developed into a numerical scheme by Parrenin et al. (2025). Chung et al. (2025) presented an inverse model based on the scheme, optimising accumulation rate, the Lliboutry thinning parameter and a mechanical ice thickness. In the companion paper, Jeaumot et al. (2026, in review) improved the basal representation and it is this version of the model that we use in this study. In this section, give an overview of the model's principle features, explain the method used to determine the flow line from DF to EDML and present the radar data along the flow line which was used to constrain the model.

2.1 Model

We use a 2.5D inverse flow model, which is presented by Jeaumot et al. (2026, in review). Here, we summarise the key aspects of the model and refer to Jeaumot et al. (2026, in review) and previous publications (Parrenin and Hindmarsh, 2007; Parrenin et al., 2025; Chung et al., 2025) for more detailed explanations. A 2.5D model considers both vertical and horizontal ice flow

https://doi.org/10.5194/egusphere-2026-4351
Preprint. Discussion started: 28 September 2026

and by using a flow tube width, it also takes into account lateral flow divergence. The model is constrained by isochrones (dated IRHs) from radar surveys.

The model uses a coordinate system described by Parrenin and Hindmarsh (2007) which is particularly efficient as in this coordinate system, ice particle trajectories are linear and therefore straight forward to calculate. The forward model was then developed by Parrenin et al. (2025). It uses input parameters and boundary conditions to calculate the ice flux and produce an age field from which modelled ages at the depths of observed isochrones can be determined. In the inverse model presented by Chung et al. (2025), a cost function evaluates the misfit between the modelled and observed isochrone ages (Eq. 2 from Chung et al., 2025). It finds the best-fit parameters to minimise this cost function and therefore the misfit. Chung et al. (2025) optimised steady accumulation rate $\bar{a}$, the Lliboutry thinning parameter p and a mechanical ice thickness H_m (first presented by Chung et al., 2023). Jeaumot et al. (2026, in review) then improved on this by optimising a Δ parameter instead of H_m, in order to account for basal melting and stagnant ice.

Steady accumulation $\bar{a}$ is the average over the whole time period considered, with variations then being taken from DF2021 (Oyabu et al., 2022) for depth $\leq$ 2150 m and a combined DFO2006+AICC2012 chronology (Dome Fuji Ice Core Project Members, 2017) for depths $>$ 2150 m. The horizontal shape function takes the form of the Lliboutry profile (Lliboutry, 1979),

$$\omega(\zeta) = 1 - \frac{p+2}{p+1}(1-\zeta) + \frac{1}{p+1}(1-\zeta)^{p+2}, \tag{1}$$

which depends on the Lliboutry parameter p. Changing the value of p modifies the shape of the Lliboutry profile such that increasing p makes Eq. 1 more linear.

In previous work, optimising the mechanical ice thickness H_m allowed for the inference of either a layer of stagnant basal ice or a basal melt rate depending on it's value relative to the ice thickness observed in the radar (H_{obs}, Chung et al., 2025, 2023). However, this method necessitated truncating the thinning function where melting occurred, leading to unphysical particle trajectories and some loss in the value of optimising p. Jeaumot et al. (2026, in review) do not directly optimise H_m to avoid truncation. They instead optimise a new Δ parameter, which has a different effect when greater or less than zero. When $\Delta < 0$, there is a layer of stagnant ice of thickness $-H_{obs}\Delta$ and basal melting $m = 0$. When $\Delta \geq 0$, the basal melt rate is $m = \bar{a}\Delta$, $H_m = H_{obs}$ and therefore, there is no stagnant ice. This more direct inversion of melt rate produces more physically robust thinning functions and particle trajectories. More details on the implementation of the Δ parameter can be found in Jeaumot et al. (2026, in review).

2.2 Flow tube

The 2.5D model requires a flow tube width in order to account for divergence. We determine the flow line from DF to EDML using surface elevation from REMA (Reference Elevation Model of Antarctica, Howat et al., 2019). We select a point downstream (in this case EDML), and find the local slope direction for that point. The direction of the steepest upward slope is then followed the distance of one step (10 km). Then the process is repeated so that the steepest slope is followed all the way to DF. The resultant line then becomes the central flow line (Figure 1). This process was repeated for two points 20 km either side of the EDML to produce two further flow lines. The distance between the two adjacent flow lines gives us the flow tube width.

https://doi.org/10.5194/egusphere-2026-4351
Preprint. Discussion started: 28 September 2026

Once the width was below 200 m, too low for the resolution of the elevation map, the flow lines were then reset to 40 km apart. The flow tube width was then normalised to its widest point (at EDML).

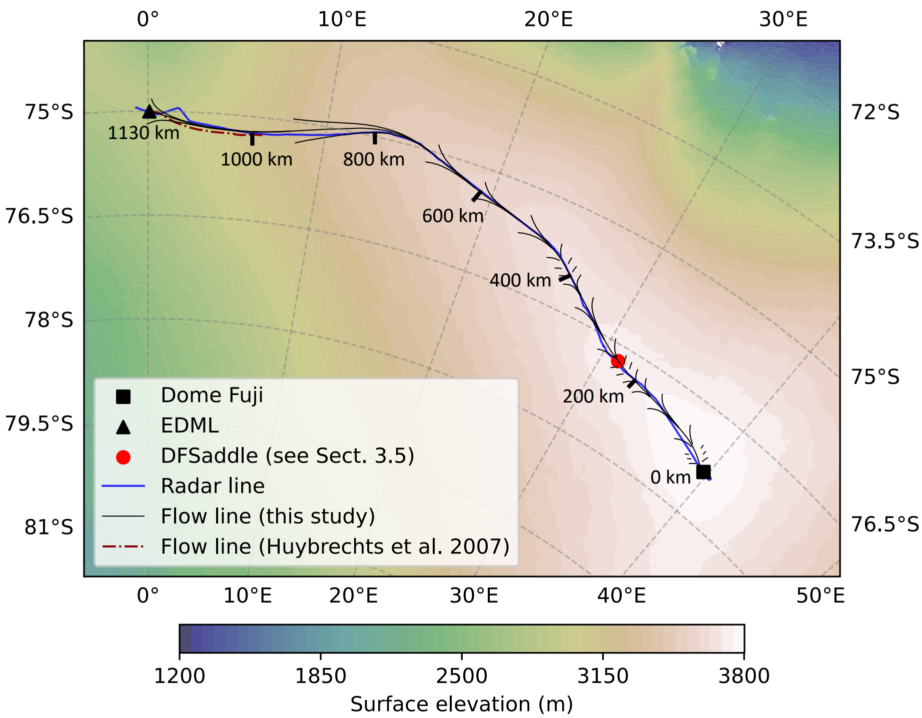

Figure 1. DF–EDML flow line. Coloured contours correspond to surface elevation (REMA Howat et al. (2019)). The black lines show the flow lines, which were restarted at a distance of 20 km either side of the central flow line each time the flow tube width decreased below 200 m. Ticks and corresponding labels mark the distance along the flow line from DF to EDML, and correspond to the distance axis in Figs 3, 4, 5 and 6.

2.3 Data

In order to constrain the 2.5D model we use IRHs along multiple radar transects that when connected, follow the approximate flow line from DF to EDML. This is known as a “stacked radar line" (blue in Fig. 2), along which Steinhage et al. (2013) presented eight IRHs. These IRHs were dated to 4.7–72.4 ka with the deepest being the oldest IRH that could be continuously traced from DF to EDML.

As the model is more stable with more and deeper isochrones, in this work we traced five further IRHs that, although they did not reach all the way to EDML, helped to constrain the fit in the upstream DF end of the flow line. Three of the new IRHs were traced as far as possible along the full stacked radar line and reach a point where they were no longer visible (end point in Table 1).

https://doi.org/10.5194/egusphere-2026-4351
Preprint. Discussion started: 28 September 2026

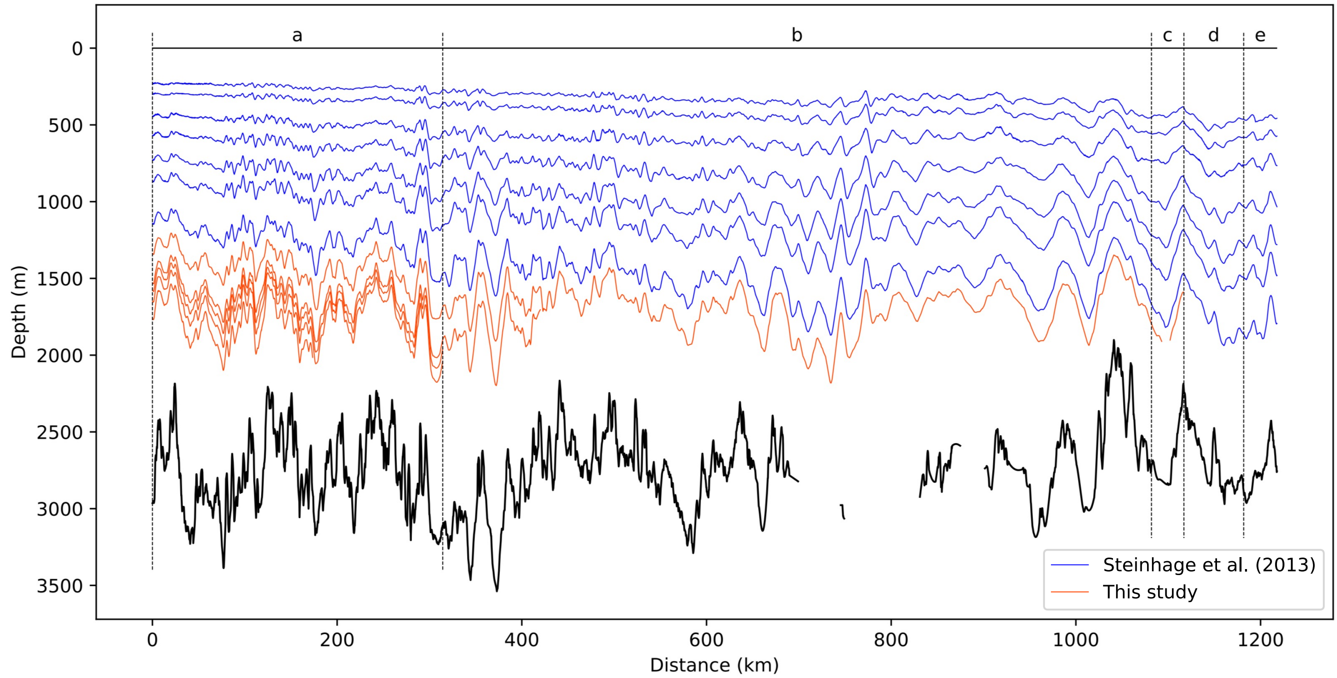

Figure 2. IRHs traced from DF (5 km) to EDML (1195 km) on the stacked radar line. The black bedrock and blue IRHs are from Steinhage et al. (2013), orange IRHs were traced as part of this study. Labelled sections come from different radar transects **a)** 2003 survey - line 3141, **b)** 1999 survey - line 3136, **c)** 1999 survey - line 3132, **d)** 1999 survey - line 3112, **e)** 2002 survey - line 3150 (for full details, see Steinhage et al., 2013). Note that these distances are not the same as the flow line distances in subsequent figures as the flow line and stacked radar line do not follow exactly the same path (see Fig. 1)

All IRHs, including those from Steinhage et al. (2013), were converted from two-way travel time to depth using the electromagnetic wave speed in ice of 168.5 m μs^{-1} (Winter et al., 2017) and a firn correction of 13 m. The IRHs were dated using the DF2021 ice core chronology (Oyabu et al., 2022). The ages of the upper eight IRHs in Table 1 therefore differ slightly from Steinhage et al. (2013), who used the Watanabe et al. (2003) chronology. There is a section of the stacked radar line where the bed could not be traced between 700–830 km distance, and a smaller section between 875–900 km.

The stacked radar line does not follow the flow line exactly, therefore we must map the IRHs onto the flow line so they can be used as model constraints. We map the IRHs by finding the intersection between a line perpendicular to the instantaneous flow line direction and the stacked radar line, as done in Chung et al. (2025).

3 Results and interpretation

Here we present the results for the 2.5D model applied to the DF–EDML flow line. The flow line goes from the summit of the dome (0 km) passing through the DF ice core site at 5 km and ending at the EDML site at 1130 km. We first look at the flow

https://doi.org/10.5194/egusphere-2026-4351
Preprint. Discussion started: 28 September 2026

IRH name	TWT at DF (ns)	Depth at DF (m)	Age (ka)	Age unc (±ka)	End point (km)
DF–EDML_1	1692	156	4.3	0.4	1218
DF–EDML_2	2575	230	7.0	0.5	1218
DF–EDML_3	3424	301	9.5	0.5	1218
DF–EDML_4	5209	452	15.4	0.9	1218
DF–EDML_5	6737	581	23.9	1.6	1218
DF–EDML_6	8782	753	37.0	1.8	1218
DF–EDML_7	10635	909	47.9	2.2	1218
DF–EDML_8	14278	1216	72.7	3.7	1218
DF–EDML_9	16780	1427	89.5	4.0	1117
DF–EDML_10	18985	1612	108.1	4.4	420
DF–EDML_11	19692	1672	114.9	4.8	314*
DF–EDML_12	20479	1738	122.0	4.0	314*
DF–EDML_13	22146	1879	131.7	4.7	173

Table 1. IRHs traced along the stack radar line with ages determined using the DF2021 chronology (Oyabu et al., 2022). IRHs numbered 1 to 8 were traced by Steinhage et al. (2013) and IRHs numbered 9 to 13 were traced in this study. The end point indicates the distance at which the isochrone could no longer be traced. *IRHs were traced only to the end of transect **a)** in Fig. 2 and may extend further along the stacked radar line.

line as a whole and then focus on the EDML drill site and Dome Fuji Saddle (DFS), another potentially interesting site for an ice core.

3.1 Inferred parameters

We first look at the values of the inferred parameters along the flow line to assess the performance of the model. Figures 3a, b and c show best-fit parameters found by the model for $\bar{a}$, p and Δ, respectively. m and stagnant ice thickness which are inferred from Δ, are also shown in Fig 3d (see Sect. 2.1).

Fig 3a shows the accumulation rate increasing from approximately 0.02 m yr^{-1} at DF to 0.05 m yr^{-1} moving towards the coast, as would be expected (Fujita et al., 2011). There is a decrease in accumulation from 700–900 km, likely due to the flow line becoming more parallel to the coast along this section. Accumulation rate is constrained by isochrones downstream of any given point. Since there are no isochrones beyond the end of the flow line, the accumulation rate is ill-constrained and becomes significantly more noisy in the last 300 km.

The value of p is generally between 5 and 10 (Fig. 3b). This is lower than the values around DC from the same model (Chung et al., 2025), meaning that the thinning function is less linear. This may be because the isochrones do not cover such a large

https://doi.org/10.5194/egusphere-2026-4351
Preprint. Discussion started: 28 September 2026

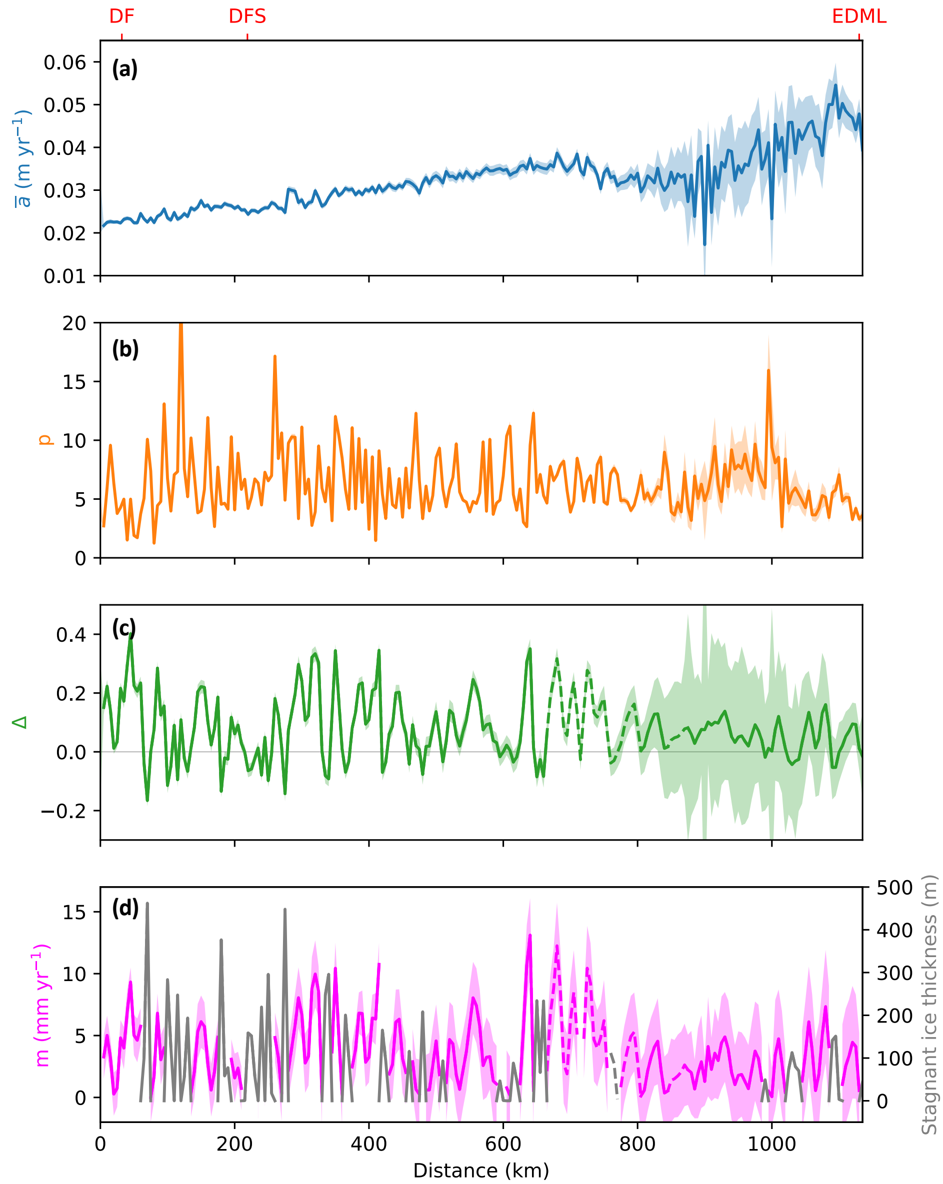

Figure 3. Inferred parameters along the DF–EDML flow line. Shaded colours show uncertainties in corresponding parameter; **a)** steady accumulation rate; **b)** p Lliboutry thinning parameter; **c)** Δ parameter; **d)** melt rate with the left hand axis (pink) and stagnant ice with the right hand axis (grey). The dashed lines in **c)** and **d)** shows results inferred using Bedmachine bed data rather than radar observations. Red labels at the top denote DF: Dome Fuji ice core site, DFS: Dome Fuji Saddle (Discussed in Sect. 3.5) and EDML: EPICA Dronning Maud Land ice core (Discussed in Sect. 3.4)

fraction of the ice thickness so the thinning function is not as well constrained along the deeper part of the DF–EDML flow line.

https://doi.org/10.5194/egusphere-2026-4351
Preprint. Discussion started: 28 September 2026

Figure 3c shows how Δ changes along the flow line. Where $\Delta > 0$, there is basal melting and where $\Delta < 0$, there is stagnant ice. The uncertainty is relatively low in the first 800 km of the flow line, then dramatically increases downstream. This area is predominantly basal melting and coincides with increased $\bar{a}$ uncertainty (Fig. 3a).

Figure 3d shows basal melt rate and stagnant ice thickness. Due to the Δ parametrisation, only one of these quantities can be non-zero. It can be seen that when comparing with the bedrock topography (Fig. 4), areas of stagnant ice occur on bedrock peaks and slightly downstream of them. Basal melting is higher in troughs, varying up to 15 mm yr^{-1}, for most of the flow line (distances < 800 km in Fig. 3). For the remainder of the flow line (distances > 800 km), the melt rate is generally below 5 mm yr^{-1}. At distances 675–805 km and 875–900 km along the flow line, there is no available observed bed in the stacked radar line used in this study (Fig. 2). Therefore, we have extracted the bed from BedMachine (Morlighem et al., 2020, dashed black line in Fig 4) as it is required for the Δ parametrisation (Jeaumot et al., 2026, in review). The BedMachine bed is used to fill observation gaps in order to tentatively infer the melt rate and stagnant ice thickness in this part of the flow line (dashed pink and dashed grey in Fig. 3d). The results suggest the melt rate is lower from around 800 km along the flow line, though we do not interpret this further due to the inherent uncertainty in using multiple data sources.

3.2 Age of ice

Figure 4 shows the age–depth relationship throughout the ice sheet along the flow line. The modelled isochrones (black) agree reasonably well with the observed isochrones (white). At distances 675–805 km and 875–900 km, the gaps are filled with BedMachine bed data (Morlighem et al., 2020, dashed black line). Along most of the flow line, the age of ice near the bed is relatively low for the East Antarctic Plateau (<500 ka) due to basal melting (see Sec. 3.1). Figure 4 shows an area of old ice occurring on a bedrock mountain around 200–250 km (discussed in Sect. 3.5), where there is a patch of stagnant ice filling the slight dip between mountains (Fig. 3d).

3.3 Ice particle trajectories

The particle trajectories along the flow line are shown in Fig. 5. In the upstream part of the flow line (distance <600 km), the trajectories tend to reach bedrock around 30 km downstream of their deposition location. This is due to a combination of strong lateral flow divergence and significant basal melting. Basal melting draws the ice particles down so they have a more direct trajectory towards the bedrock. Downstream, where lateral divergence is lower, trajectories rise over bedrock highs and particles travel further horizontally in the deeper parts of the ice sheet before reaching the bed.

3.4 EDML ice core site

Figure 6a shows the modelled age at the EDML ice core site (solid blue line). It agrees well with the EDML1 ice core chronology (Ruth et al., 2007, dotted blue line) and the modelling by Huybrechts et al. (2007, dashed blue line), to a depth of around 2000 m. The age then begins to deviate slightly and suggest that deeper ice is younger than these previous studies. The DF ice core chronologies (Oyabu et al., 2022; Dome Fuji Ice Core Project Members, 2017) were used for dating the

https://doi.org/10.5194/egusphere-2026-4351
Preprint. Discussion started: 28 September 2026

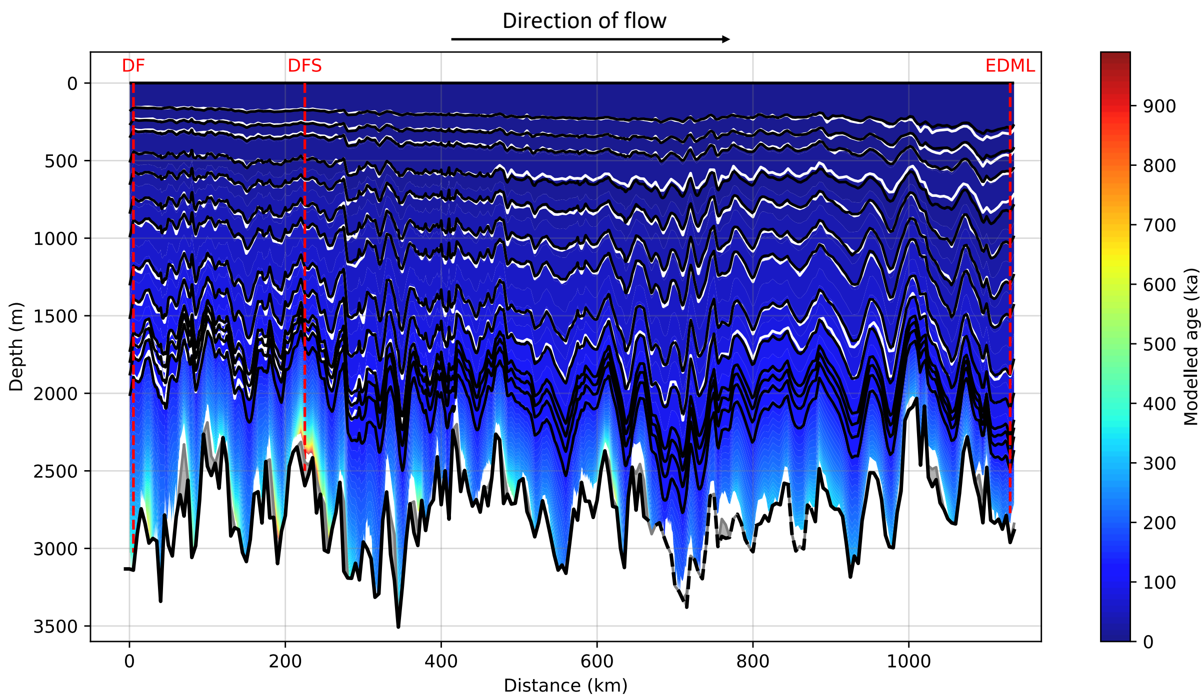

Figure 4. The modelled age–depth relationship along the DF–EDML flow line. The bold black line is the observed bedrock from radar data and the dashed black line represents the bedrock gaps filled in using BedMachine (Morlighem et al., 2020). The white lines show the observed isochrones and the black lines overlaid show the modelled isochrones. The grey areas just above the bed show stagnant ice. Both DF and EDML ice cores are marked at 5 km and 1130 km respectively. DFS (discussed in Sect. 3.5) is marked at 225 km. The modelled age of the ice is represented by the colour gradient and corresponding colourbar. The arrow at the top shows the horizontal direction of flow from DF to EDML.

IRHs and for the temporal factor which accounts for variations in accumulation (see Chung et al., 2023, Eq. 1). Comparing the thinning functions from this study and Huybrechts et al. (2007), they are relatively similar in terms of linearity. However, specific deviations from linearity caused by the bedrock upstream are offset. For example, a major deviation from linearity in the thinning function occurs in both this study and Huybrechts et al. (2007) at around 2085 m and 1750 m depth respectively. When looking at the ice origins (red solid and dotted lines respectively) at these depths, we can see that in both cases, the ice particles originate from a distance of around 1070 km along the radar line or 60 km upstream of EDML. From Fig. 5, there is a clear bedrock rise at this distance, which causes particle trajectories to rise before moving down again towards EDML.

The ice particle origins do not agree as closely, as they begin to deviate at around 1000 m depth. This study suggests that the deepest ice at EDML comes from 130 km upstream, as opposed to almost 200 km upstream from Huybrechts et al. (2007).

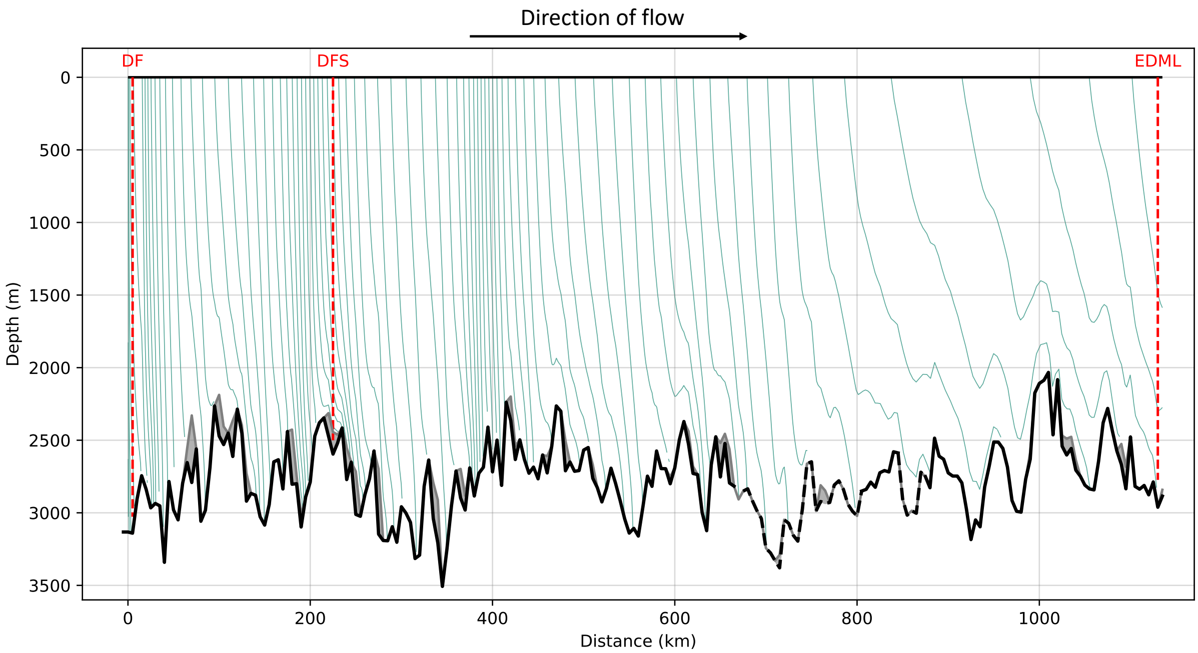

Figure 5. Thin green lines show particle trajectories. The thick black line is the observed bedrock and purple is the inferred bedrock. The dashed black line is the bed taken from BedMachine which fills in the gaps in the radar. The arrow at the top shows the horizontal direction of flow from DF to EDML.

3.5 Potential Old Ice: Dome Fuji Saddle

The areas with the oldest ice clearly occur on bedrock highs (Fig. 4). We identify one such area at 210–235 km where the age of the deepest ice is the oldest modelled along the flow line. On the surface this area is relatively flat (red circle in Fig 1), we therefore label it Dome Fuji Saddle (DFS).

Fig 6b shows the age-depth profile at 225 km along the flow line – a location particularly promising for old ice. The ice sheet thickness at this location is 2596 m and there is a modelled stagnant ice layer 152 m thick. The maximum age is defined as the depth at which the age density of ice becomes >20 kyr m^{-1} (Fischer et al., 2013). At DFS this occurs at a depth of 2382 m with a maximum age of 1.05 Ma with this ice coming from around 25 km upstream. The p value of the thinning function is around 5.

4 Discussion

In this work, we apply a 2.5D ice flow model to the DF–EDML flow line. Here we discuss the model and data limitations and how results compare to the literature.

https://doi.org/10.5194/egusphere-2026-4351
Preprint. Discussion started: 28 September 2026

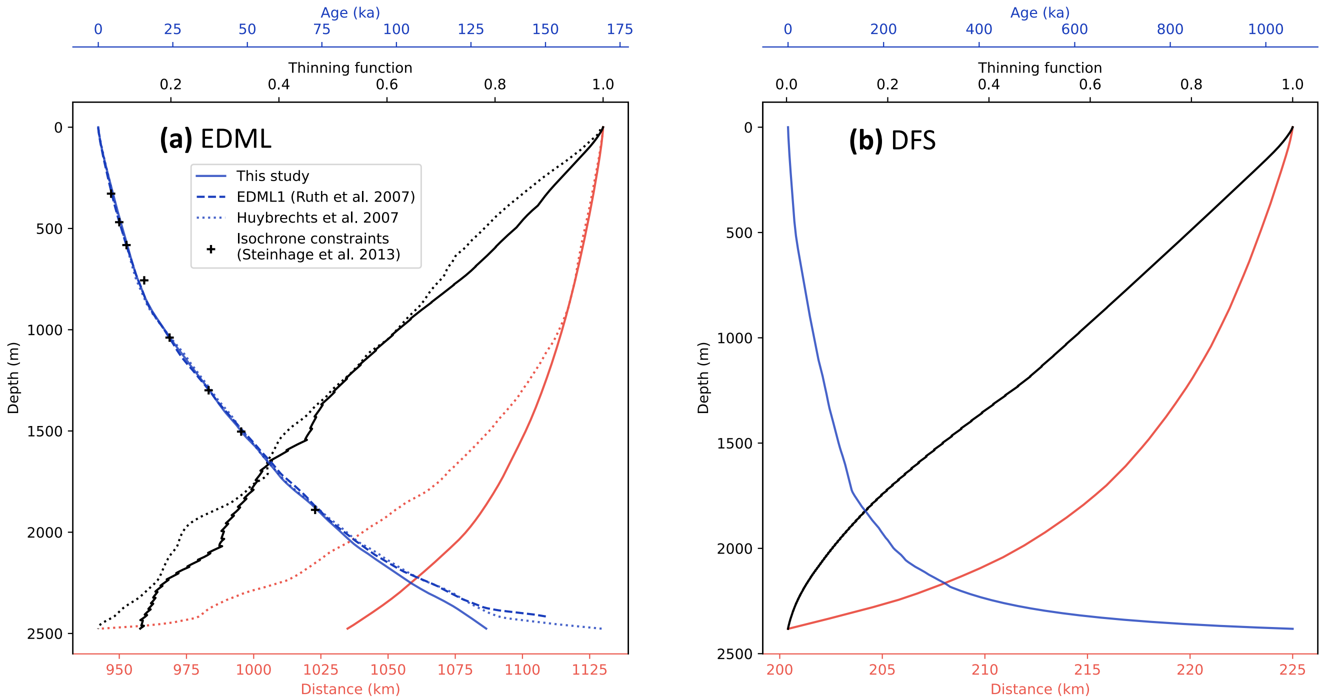

Figure 6. a) Age, thinning and ice particle origin at EDML from this study and literature (solid lines): modelled age (blue), ice equivalent thinning (black) and ice particle origin (red) for the EDML ice core. Each line is plotted against depth and an x-axis with the corresponding colour. For example, ice at 1500 m depth is 50 ka and originates from a distance of 1100 km along the flow line (30 km upstream of the EDML core, which is at distance 1130 km). The dotted lines show the results from Huybrechts et al. (2007) and the dashed blue line shows the EDML1 chronology from Ruth et al. (2007). Black crosses show the isochrones used to constrain the model in this study marked on the age–depth scale (Fig 2). **b)** Modelled age (blue), thinning (black) and ice particle origin (red) at DFS (Dome Fuji Saddle, distance 225 km along flow line) from this study only.

4.1 Model limitations

As mentioned in Sect. 2, the forward model uses a highly efficient coordinate system (Parrenin and Hindmarsh, 2007). Currently, the conversion from this coordinate system to an (x,z) grid for comparison to observed isochrones is done through linear interpolation. However, a quadratic interpolation would more closely represent the physical system. For now, it would be too computationally expensive to implement, given that the interpolation is by far the most time consuming element of the model.

As this flow line is much longer than the DC–LDC flow line, previously investigated using this model (Chung et al., 2025; Jeaumot et al., 2026, in review), the computation time and memory required increased dramatically. Therefore it would now be beneficial to parallelise the code so that it can run more efficiently on multiple cores. This would also enable the model to run for different sets of parameters simultaneously, perhaps at a higher resolution, to find the optimal combination of parameters. Another possible improvement would be to use an automatic differentiation method, such as JAX (The JAX authors, 2024),

https://doi.org/10.5194/egusphere-2026-4351
Preprint. Discussion started: 28 September 2026

which would make the least-squares method find a best-fit solution more efficiently than the current numerical finite difference Jacobian, which is more of a brute force method.

The introduction of the optimised Δ parameter by Jeaumot et al. (2026, in review) has improved the physical representation over its previous iteration (Chung et al., 2025). Particle trajectories are more realistic and do not produce unphysical paths passing through bedrock, generating "accreted ice" areas (Chung et al., 2025). However, one disadvantage is that the Δ parameterisation requires a bedrock depth observation (H_{obs}) along the entire flow line, which was not available in this case (Fig. 2), necessitating the use of BedMachine to fill the gaps. In a model optimising the mechanical ice thickness, H_{obs} is necessary for determining melt rates or stagnant ice thickness, but the age field can be modelled without H_{obs}. A full discussion of the improvements and limitations brought by the Δ parameterisation can be found in the companion paper Jeaumot et al. (2026, in review)

We use the surface elevation slope to determine the width of the flow tube. However, this method may not correctly estimate the lateral divergence which could explain the shorter distance travelled by particles to EDML, relative to Huybrechts et al. (2007) (Fig. 6a). Attempts were made to use surface velocity to determine the flow tube width, but due to the low resolution of measurements and low velocities, it was not possible to determine a continuous flow tube from DF to EDML. Passalacqua et al. (2016) carried out a study on the suitability of a 2.5D model in areas with dome or divide flow characteristics. They found that due to the Raymond effect (Raymond, 1983), flow tube walls are not perfectly vertical as is assumed in our work. However, in order to determine more physically realistic flow tube walls, there would need to be measurements of velocities inside the ice sheet. Moreover, our model assumes the temporal factor is the same along the whole flow line, but that might not be the case: the temporal variations of accumulation at DF and EDML may be slightly decoupled. The results of the combined potential sources of error would affect the shape of particle trajectories and perhaps the horizontal distance travelled by ice particles.

4.2 Observational data limitations

As the IRHs were dated by linking them to the DF ice core, the modelled EDML profile is independent of the EDML1 chronology. This means that if there are particularities in DF chronology (Oyabu et al., 2022) due to local glaciological conditions, they would be transferred to this modelled EDML chronology.

To increase the reliability of the result, it would be beneficial to have more deeper isochrones to constrain the lower portion of the ice sheet. There are a couple of isochrones that may continue further along the line than traced but could not be due to time constraints (Table 1). However, it is not possible to trace deeper isochrones in current radar data so a new radar survey would have to be conducted. In Fig. 4, we compare the observed isochrones (white lines) with modelled isochrones (black lines overlaid). The fourth modelled isochrone ($\sim$ 500m depth at DF) matches well with the observation to a distance of about 450 km. After this point, the modelled isochrone is systematically deeper than the observation, suggesting that there could be an issue with the radar data itself. In this case, the IRH detected by the radar system is actually a combination of multiple horizons. The ratio of accumulation rates at DF and EDML changed over the last glacial period meaning that the combination of horizons is different at different areas along the flow line. This means that what seems to be a continuous IRH in the radargram is actually an artefact and not a true representation of an isochrone.

https://doi.org/10.5194/egusphere-2026-4351
Preprint. Discussion started: 28 September 2026

In Fig. 6a, the modelled age scale for EDML (solid blue line), begins to deviate from previous modelling and ice core measurements at around 2000 m, just below the deepest isochrone constraint. As the EDML ice core provides deeper constraints than the radar isochrones, a further step would be to include EDML dated tie-points as additional constraints in the cost function. This would correct the modelled age scale at EDML in the deeper part and provide better constrained best-fit parameters. However, EDML could no longer be used for validation in this case.

In the distance intervals 675–805 km and 875–900 km, there is no data for the bed in the radargrams presented by Steinhage et al. (2013). Therefore we have filled these gaps using the bedrock elevation dataset BedMachine (Morlighem, 2022) as it is required for the model. Melt rates, stagnant ice and particle trajectories a distance >675 km may be inferred using the BedMachine interpolated values for the bedrock. As these data comes from a different source to the isochrones used as constraints, the uncertainty is difficult to quantify. Therefore, we recommend caution with further interpretation of the melt rates and stagnant ice thicknesses in this section of the flow line.

4.3 Comparison to literature

This 2.5D model has previously been applied to the DC–LDC flow line by Chung et al. (2025) where the benefits over a 1D model were limited due to the low horizontal flow in that area. In this work, we apply the model to an area where the properties of a 2.5D are more relevant due to increasing horizontal advection along the flow line from DF to EDML. The 2.5D model used in this study is an alternative method to the 3D model presented by Huybrechts et al. (2007). Their model has higher order processes but lower spatial resolution and was not constrained by observational data.

The best-fit values for steady accumulation are presented in Fig. 3a and show that generally accumulation increases closer to the coast. There is a decrease in accumulation from 700–900 km, possibly due to the fact that the flow line at this point turns slightly off of the main divide. In this area, the flow line follows a path more parallel to the coastline. Therefore, the accumulation rate stops increasing. Fujita et al. (2011) determined accumulation along the DF–EDML flow line using measurements from shallow ground-penetrating radar. They found similar trends to this study, with a low, relatively stable accumulation rate in the first 400 km, gradually increasing towards the coast. They also observed high fluctuations in the second half of the flow line and the slight decrease between 700-900 km. The agreement with Fig. 3a supports the methods used to infer the accumulation rate in this study.

Figure 3d shows the thickness of stagnant ice. In Figs. 4 and 5, it is clear that stagnant ice occurs on top of and slightly downstream of bedrock rises. Some patches of stagnant ice form almost as a downstream shadow of rises, for example at distances of 340 km and 650 km. Hindmarsh et al. (2006) investigated the difference between isochrones that drape over the basal topography, following its approximate shape and isochrones that override it, lying relatively flat over bedrock rises. The presence of stagnant ice may therefore indicate overriding isochrones at certain locations along the flow line. This effect is similar to that observed at LDC (Chung et al., 2025; Jeaumot et al., 2026, in review) where trajectories rise over a sudden bedrock peak and do not immediately fall with topography. The model suggests that there is a shear layer between the ice passing above, following the trajectories and the ice trapped on the downstream side of the mountain. Initial analysis of the Beyond EPICA ice core at LDC would seem to support the existence of a shear layer at the approximate depth of the modelled

https://doi.org/10.5194/egusphere-2026-4351
Preprint. Discussion started: 28 September 2026

stagnant ice (Westhoff et al., 2026). However, whether the same phenomenon occurs along this flow line from DF to EDML is unclear and would require higher resolution modelling and more extensive radar focussing on one of these areas.

The surface velocity near EDML was measured by Wesche et al. (2007) using Global Navigation Satellite System (GNSS) measurements to monitor a network of stakes. They found the surface velocity at the EDML drill site to be 0.756 m yr^{-1} and at a site 15 km upstream, it was 0.963 m yr^{-1}. In this study, the modelled surface velocity was 0.73 m yr^{-1} and 0.9 m yr^{-1} at these two locations respectively, showing remarkably good agreement with observations. Huybrechts et al. (2007) also obtain a value of exactly 0.73 m yr^{-1} at EDML, but the origin of the deepest ice is very different. At EDML, we find that the oldest ice originates from around 130 km upstream, whereas this value is almost 200 km for the Huybrechts et al. (2007) study. It is therefore difficult to draw conclusions from the comparisons with the surface velocity measurements as an indicator of realistic flow trajectories deep in the ice sheet.

Figure 6a shows the comparison of modelled results at EDML with those in the literature. The age–depth profile is similar to those presented by Ruth et al. (2007) and Huybrechts et al. (2007) down to 2000 m. The lack of deep isochrone constraints may go some way towards explaining why the age scale modelled in this study deviates slightly from the Huybrechts et al. (2007) modelling study and the chronology obtained through ice core measurements (Ruth et al., 2007). Radar surveys at EDML found an echo-free zone (EFZ) from a depth of 2100 m until the bedrock at around 2800 m (Drews et al., 2009). It was assumed that, as no features were detectable in the radar, the ice was disturbed in the EFZ. However, the deepest detectable palaeoclimatic signal in the EDML ice core was found at 2416 m, about 50% of the thickness of the EFZ (Ruth et al., 2007). The modelled age scale in this study in the EFZ does not agree well with the established chronology, perhaps indicating that ice flow behaviour in this zone is more complex than this model allows for.

At the base of EDML, there is high anisotropy, which is thought to be a result of changing crystal-orientation fabric (Eisen et al., 2007). In order to account for this, Huybrechts et al. (2007) used the Glen flow enhancement factor. The model used in this study does not directly consider anisotropy. However, by the fitting of the p parameter in the Lliboutry vertical velocity profile (Eq. 1), some effects of anisotropy can be accounted for (Sect. 2).

This model has steady geometry which assumes that the ice sheet thickness has not changed over the period of time considered. Moreover, the spatial origin of ice particles within the ice sheet is strongly influenced by the variations of flow tube width along the flow line, which is calculated from the steepest slope of the surface. The altitude may also not be the same as today which adds uncertainty when applying this kind of modelled correction to the palaeoclimate record present in the EDML ice core.

4.4 Old ice prospects

The oldest ice along the flow line tends to occur on bedrock mountain (Fig 4). The mountain rises slow down ice flow, making the ice sheet thicker. Once the ice sheet is too thick, it insulates the geothermal heat flux, causing basal melting. The ice sheet therefore finds an equilibrium between these two factors. The area of DFS (Sect. 3.5) was identified as potentially having the oldest ice along the flow line (Fig. 6). This area was already highlighted by Van Liefferinge et al. (2018) and Karlsson et al. (2018) in their studies using thermodynamical modelling and geothermal heat flux (GHF) to find areas where the ice sheet

https://doi.org/10.5194/egusphere-2026-4351
Preprint. Discussion started: 28 September 2026

is thick enough to have old ice but GHF is low enough that basal melting is unlikely. Although this exact location was not modelled by Wang et al. (2023), they also found that the area is promising for old ice when considering the basal age and age density according to a 1D inverse model. In this study, the maximum age of ice occurs at the bed and is around 1 Ma. It is important bare in mind that the resolution of this study's inverse model is around 5 km. The spatial resolution of the radar data is much higher than the modelling done here. Therefore, the model could be rerun with only the first 250 km along the flow line which would allow much higher resolution. This would give more accurate information on the age-depth profile at DFS. However the deepest isochrone in the current flow line radar data is 131.7 ka (Table 1) which is relatively shallow compared to other studies using similar methods (Chung et al., 2025; Wang et al., 2023). Therefore, to more definitively model the basal age in this area, a deeper penetrating radar survey would need to be conducted.

5 Conclusions

We applied a 2.5D inverse model to the DF–EDML flow line using radar horizon as constraints. The accumulation reconstruction provided by the modelling in this study shows a general increase towards the coast following the trend found in previous studies based on observations. Our results suggest that basal melting is higher in bedrock troughs and stagnant ice occurs on or on the downstream side of bedrock peaks. We determined particle trajectories along the entire DF–EDML flow line for the first time. We find that the deepest ice at EDML originates from 130 km upstream. Compared to a more complex 3D model run focussing only on EDML, this is much closer to the ice core drill site. Modelled surface velocities around EDML agrees well with observations supporting the use of the 2.5D model in this region. We also show further evidence supporting a potential old ice drilling site, DFS, situated 225 km from the dome on a weak saddle point, hence with a quasi-vertical ice flow. Deeper radar constraints would improve the inference of basal conditions such as basal melt rate or age of the ice.

Code availability. The code is availiable here https://github.com/yevajeaumot/IsoInv2.5D

Author contributions. AC defined the flow line, traced the new radar horizons, developed the model set up and wrote the manuscript. FP and AC developed the forward and inverse models. YJ implemented the Delta parameterisation and applied the model to the flow line. OE and DS provided radar data and facilitated tracing. All co-authors read and commented on the manuscript.

Competing interests. The authors declare no competing interests.

Acknowledgements. This publication was generated in the frame of Beyond EPICA. The project has received funding from the European Union's Horizon 2020 research and innovation programme under grant agreement no. 815384 (Oldest Ice Core). It is supported by national

https://doi.org/10.5194/egusphere-2026-4351
Preprint. Discussion started: 28 September 2026

partners and funding agencies in Belgium, Denmark, France, Germany, Italy, Norway, Sweden, Switzerland, The Netherlands and the United Kingdom. Logistic support is mainly provided by ENEA and IPEV through the Concordia Station system. This publication was generated in the frame of the DEEPICE project which has received funding from the European Union's Horizon 2020 research and innovation programme under the Marie Sklodowska-Curie grant agreement no. 955750. The opinions expressed and arguments employed herein do not necessarily reflect the official views of the European Union funding agency or other national funding bodies. This is Beyond EPICA publication number XX.

https://doi.org/10.5194/egusphere-2026-4351
Preprint. Discussion started: 28 September 2026

References

Albrecht, T., Winkelmann, R., and Levermann, A.: Glacial-cycle simulations of the Antarctic Ice Sheet with the Parallel Ice Sheet Model (PISM)-Part 2: Parameter ensemble analysis, The Cryosphere, 14, 633–656, ISSN 19940424, https://doi.org/10.5194/tc-14-633-2020, 2020a.

Albrecht, T., Winkelmann, R., and Levermann, A.: Glacial-cycle simulations of the Antarctic Ice Sheet with the Parallel Ice Sheet Model (PISM)-Part 1: Boundary conditions and climatic forcing, The Cryosphere, 14, 599–632, ISSN 19940424, https://doi.org/10.5194/tc-14-599-2020, 2020b.

Ashmore, D. W., Bingham, R. G., Ross, N., Siegert, M. J., Jordan, T. A., and Mair, D. W. F.: Englacial Architecture and Age–Depth Constraints Across the West Antarctic Ice Sheet, Geophysical Research Letters, 47, https://doi.org/10.1029/2019GL086663, 2020.

Bingham, R. G., Bodart, J. A., Cavitte, M. G. P., Chung, A., Sanderson, R. J., Sutter, J. C. R., Eisen, O., Karlsson, N. B., MacGregor, J. A., Ross, N., Young, D. A., Ashmore, D. W., Born, A., Chu, W., Cui, X., Drews, R., Franke, S., Goel, V., Goodge, J. W., Henry, A. C. J., Hermant, A., Hills, B. H., Holschuh, N., Koutnik, M. R., Leysinger Vieli, G. J.-M. C., MacKie, E. J., Mantelli, E., Martín, C., Ng, F. S. L., Oraschewski, F. M., Napoleoni, F., Parrenin, F., Popov, S. V., Rieckh, T., Schlegel, R., Schroeder, D. M., Siegert, M. J., Tang, X., Teisberg, T. O., Winter, K., Yan, S., Davis, H., Dow, C. F., Fudge, T. J., Jordan, T. A., Kulessa, B., Matsuoka, K., Nyqvist, C. J., Rahnemoonfar, M., Siegfried, M. R., Singh, S., Višnjević, V., Zamora, R., and Zuhr, A.: Review article: AntArchitecture – building an age–depth model from Antarctica's radiostratigraphy to explore ice-sheet evolution, The Cryosphere, 19, 4611–4655, ISSN 1994-0424, https://doi.org/10.5194/tc-19-4611-2025, 2025.

Born, A. and Robinson, A.: Modeling the Greenland englacial stratigraphy, The Cryosphere, 15, 4539–4556, ISSN 19940424, https://doi.org/10.5194/tc-15-4539-2021, 2021.

Cavitte, M. G., Blankenship, D. D., Young, D. A., Schroeder, D. M., Parrenin, F., Lemeur, E., MacGregor, J. A., and Siegert, M. J.: Deep radiostratigraphy of the East Antarctic plateau: Connecting the Dome C and Vostok ice core sites, Journal of Glaciology, 62, 323–334, ISSN 00221430, https://doi.org/10.1017/jog.2016.11, 2016.

Chung, A., Parrenin, F., Steinhage, D., Mulvaney, R., Martín, C., Cavitte, M. G. P., Lilien, D. A., Helm, V., Taylor, D., Gogineni, P., Ritz, C., Frezzotti, M., O'Neill, C., Miller, H., Dahl-Jensen, D., and Eisen, O.: Stagnant ice and age modelling in the Dome C region, Antarctica, The Cryosphere, 17, 3461–3483, https://doi.org/10.5194/tc-17-3461-2023, 2023.

Chung, A., Parrenin, F., Mulvaney, R., Vittuari, L., Frezzotti, M., Zanutta, A., Lilien, D. A., Cavitte, M. G., and Eisen, O.: Age, thinning and spatial origin of the Beyond EPICA ice from a 2.5D ice flow model, The Cryosphere, 19, 4125–4140, ISSN 19940424, https://doi.org/10.5194/tc-19-4125-2025, 2025.

Dahl-Jensen, D.: Drilling for the oldest ice, Nature Geoscience, 11, 703–704, ISSN 1752-0894, https://doi.org/10.1038/s41561-018-0241-2, 2018.

Dome Fuji Ice Core Project Members: State dependence of climatic instability over the past 720,000 years from Antarctic ice cores and climate modeling, Science Advances, 3, 1–13, ISSN 2375-2548, https://doi.org/10.1126/sciadv.1600446, 2017.

Drews, R., Eisen, O., Weikusat, I., Kipfstuhl, S., Lambrecht, A., Steinhage, D., Wilhelms, F., and Miller, H.: Layer disturbances and the radio-echo free zone in ice sheets, The Cryosphere, 3, 195–203, ISSN 1994-0424, https://doi.org/10.5194/tc-3-195-2009, 2009.

Eisen, O., Wilhelms, F., Steinhage, D., and Schwander, J.: Improved method to determine radio-echo sounding reflector depths from ice-core profiles of permittivity and conductivity, Journal of Glaciology, 52, 299–310, ISSN 0022-1430, https://doi.org/10.3189/172756506781828674, 2006.

Eisen, O., Hamann, I., Kipfstuhl, S., Steinhage, D., and Wilhelms, F.: Direct evidence for continuous radar reflector originating from changes in crystal-orientation fabric, The Cryosphere, 1, 1–10, ISSN 19940416, https://doi.org/10.5194/tc-1-1-2007, 2007.

Fischer, H., Siggaard-Andersen, M., Ruth, U., Röthlisberger, R., and Wolff, E.: Glacial/interglacial changes in mineral dust and sea-salt records in polar ice cores: Sources, transport, and deposition, Reviews of Geophysics, 45, ISSN 8755-1209, https://doi.org/10.1029/2005RG000192, 2007.

Fischer, H., Severinghaus, J., Brook, E., Wolff, E., Albert, M., Alemany, O., Arthern, R., Bentley, C., Blankenship, D., Chappellaz, J., Creyts, T., Dahl-Jensen, D., Dinn, M., Frezzotti, M., Fujita, S., Gallee, H., Hindmarsh, R., Hudspeth, D., Jugie, G., Kawamura, K., Lipenkov, V., Miller, H., Mulvaney, R., Parrenin, F., Pattyn, F., Ritz, C., Schwander, J., Steinhage, D., Van Ommen, T., and Wilhelms, F.: Where to find 1.5 million yr old ice for the IPICS "Oldest-Ice" ice core, Climate of the Past, 9, 2489–2505, ISSN 18149332, https://doi.org/10.5194/cp-9-2489-2013, 2013.

Fujita, S., Holmlund, P., Andersson, I., Brown, I., Enomoto, H., Fujii, Y., Fujita, K., Fukui, K., Furukawa, T., Hansson, M., Hara, K., Hoshina, Y., Igarashi, M., Iizuka, Y., Imura, S., Ingvander, S., Karlin, T., Motoyama, H., Nakazawa, F., Oerter, H., Sjöberg, L. E., Sugiyama, S., Surdyk, S., Ström, J., Uemura, R., and Wilhelms, F.: Spatial and temporal variability of snow accumulation rate on the East Antarctic ice divide between Dome Fuji and EPICA DML, The Cryosphere, 5, 1057–1081, ISSN 1994-0424, https://doi.org/10.5194/tc-5-1057-2011, 2011.

Gerber, T. A., Hvidberg, C. S., Rasmussen, S. O., Franke, S., Sinnl, G., Grinsted, A., Jansen, D., and Dahl-Jensen, D.: Upstream flow effects revealed in the EastGRIP ice core using Monte Carlo inversion of a two-dimensional ice-flow model, The Cryosphere, 15, 3655–3679, ISSN 19940424, https://doi.org/10.5194/tc-15-3655-2021, 2021.

Golledge, N. R., Kowalewski, D. E., Naish, T. R., Levy, R. H., Fogwill, C. J., and Gasson, E. G.: The multi-millennial Antarctic commitment to future sea-level rise, Nature, 526, 421–425, ISSN 14764687, https://doi.org/10.1038/nature15706, 2015.

Grisart, A., Casado, M., Gkinis, V., Vinther, B., Naveau, P., Vrac, M., Laepple, T., Minster, B., Prié, F., Stenni, B., Fourré, E., Steen-Larsen, H. C., Jouzel, J., Werner, M., Pol, K., Masson-Delmotte, V., Hoerhold, M., Popp, T., and Landais, A.: Sub-millennial climate variability from high-resolution water isotopes in the EPICA Dome C ice core, Climate of the Past, 18, 2289–2301, ISSN 18149332, https://doi.org/10.5194/cp-18-2289-2022, 2022.

Hindmarsh, R. C., Leysinger Vieli, G. J., Raymond, M. J., and Gudmundsson, G. H.: Draping or overriding: The effect of horizontal stress gradients on internal layer architecture in ice sheets, Journal of Geophysical Research: Earth Surface, 111, ISSN 21699011, https://doi.org/10.1029/2005JF000309, 2006.

Howat, I. M., Porter, C., Smith, B. E., Noh, M. J., and Morin, P.: The reference elevation model of Antarctica, The Cryosphere, 13, 665–674, ISSN 19940424, https://doi.org/10.5194/tc-13-665-2019, 2019.

Huybrechts, P., Rybak, O., Pattyn, F., Ruth, U., and Steinhage, D.: Ice thinning, upstream advection, and non-climatic biases for the upper 89% of the EDML ice core from a nested model of the Antarctic ice sheet, Climate of the Past, 3, 577–589, ISSN 18149332, https://doi.org/10.5194/cp-3-577-2007, 2007.

Jeaumot, Y., Parrenin, F., Chung, A., Eisen, O., Steinhage, D., Mulvaney, R., Cavitte, M. G. P., Lilien, D. A., and Capron, E.: An improved parameterisation of basal processes for age of ice modelling in the Dome C region, Antarctica, EGUsphere Preprint Repository, https://doi.org/10.5194/egusphere-2026-4174, 2026.

Jordan, T. A., Martin, C., Ferraccioli, F., Matsuoka, K., Corr, H., Forsberg, R., Olesen, A., and Siegert, M.: Anomalously high geothermal flux near the South Pole, Scientific Reports, 8, ISSN 20452322, https://doi.org/10.1038/s41598-018-35182-0, 2018.

Karlsson, N. B., Binder, T., Eagles, G., Helm, V., Pattyn, F., Van Liefferinge, B., and Eisen, O.: Glaciological characteristics in the Dome Fuji region and new assessment for "Oldest Ice", The Cryosphere, 12, 2413–2424, ISSN 19940424, https://doi.org/10.5194/tc-12-2413-2018, 2018.

Li, D., Tang, X., Chung, A., Parrenin, F., and Sun, B.: Simulated evidence for ice over 1Ma in the Dome A region, East Antarctica, EGUsphere Preprint Repository, 2026, 1–18, https://doi.org/10.5194/egusphere-2025-5165, 2026.

Lliboutry, L.: A critical review of analytical approximate solutions for steady state velocities and temperatures in cold ice sheets, in: Z. Gletscherkde. Glazialgeol., vol. 15, pp. 135–148, 1979.

Lüthi, D., Le Floch, M., Bereiter, B., Blunier, T., Barnola, J.-M., Siegenthaler, U., Raynaud, D., Jouzel, J., Fischer, H., Kawamura, K., and Stocker, T. F.: High-resolution carbon dioxide concentration record 650,000–800,000 years before present, Nature, 453, 379–382, ISSN 0028-0836, https://doi.org/10.1038/nature06949, 2008.

Morlighem, M.: MEaSUREs BedMachine Antarctica, Version 3, https://doi.org/10.5067/FPSU0V1MWUB6, 2022.

Morlighem, M., Rignot, E., Binder, T., Blankenship, D., Drews, R., Eagles, G., Eisen, O., Ferraccioli, F., Forsberg, R., Fretwell, P., Goel, V., Greenbaum, J. S., Gudmundsson, H., Guo, J., Helm, V., Hofstede, C., Howat, I., Humbert, A., Jokat, W., Karlsson, N. B., Lee, W. S., Matsuoka, K., Millan, R., Mouginot, J., Paden, J., Pattyn, F., Roberts, J., Rosier, S., Ruppel, A., Seroussi, H., Smith, E. C., Steinhage, D., Sun, B., Broeke, M. R. d., Ommen, T. D., Wessem, M. v., and Young, D. A.: Deep glacial troughs and stabilizing ridges unveiled beneath the margins of the Antarctic ice sheet, Nature Geoscience, 13, 132–137, ISSN 17520908, https://doi.org/10.1038/s41561-019-0510-8, 2020.

Obase, T., Abe-Ouchi, A., Saito, F., Tsutaki, S., Fujita, S., Kawamura, K., and Motoyama, H.: A one-dimensional temperature and age modeling study for selecting the drill site of the oldest ice core near Dome Fuji, Antarctica, The Cryosphere, 17, 2543–2562, ISSN 19940424, https://doi.org/10.5194/tc-17-2543-2023, 2023.

Oyabu, I., Kawamura, K., Buizert, C., Parrenin, F., Orsi, A., Kitamura, K., Aoki, S., and Nakazawa, T.: The Dome Fuji ice core DF2021 chronology (0–207 kyr BP), Quaternary Science Reviews, 294, ISSN 02773791, https://doi.org/10.1016/j.quascirev.2022.107754, 2022.

Parrenin, F. and Hindmarsh, R.: Influence of a non-uniform velocity field on isochrone geometry along a steady flowline of an ice sheet, Journal of Glaciology, 53, 612–622, ISSN 00221430, https://doi.org/10.3189/002214307784409298, 2007.

Parrenin, F., Chung, A., and Martín, C.: age_flow_line-1.0: a fast and accurate numerical age model for a pseudo-steady flow tube of an ice sheet, Geoscientific Model Development, 18, 8203–8216, ISSN 1991-9603, https://doi.org/10.5194/gmd-18-8203-2025, 2025.

Passalacqua, O., Gagliardini, O., Parrenin, F., Todd, J., Gillet-Chaulet, F., and Ritz, C.: Performance and applicability of a 2.5-D ice-flow model in the vicinity of a dome, Geoscientific Model Development, 9, 2301–2313, ISSN 19919603, https://doi.org/10.5194/gmd-9-2301-2016, 2016.

Petit, J.-R. and Raynaud, D.: Forty years of ice-core records of CO2, Nature, 579, 505–506, ISSN 0028-0836, https://doi.org/10.1038/d41586-020-00809-8, 2020.

Raymond, C. F.: Deformation in the Vicinity of Ice Divides, Journal of Glaciology, 29, 357–373, ISSN 0022-1430, https://doi.org/10.3189/s0022143000030288, 1983.

Ruth, U., Barnola, J. M., Beer, J., Bigler, M., Blunier, T., Castellano, E., Fischer, H., Fundel, F., Huybrechts, P., Kaufmann, P., Kipfstuhl, S., Lambrecht, A., Morganti, A., Oerter, H., Parrenin, F., Rybak, O., Severi, M., Udisti, R., Wilhelms, F., and Wolff, E.: "EDML1": A chronology for the EPICA deep ice core from Dronning Maud Land, Antarctica, over the last 150 000 years, Climate of the Past, 3, 475–484, ISSN 18149332, https://doi.org/10.5194/cp-3-475-2007, 2007.

https://doi.org/10.5194/egusphere-2026-4351
Preprint. Discussion started: 28 September 2026

Siegert, M. J. and Hodgkins, R.: A stratigraphic link across 1100 km of the antarctic ice sheet between the Vostok ice-core site and Titan Dome (near South Pole), Geophysical Research Letters, 27, 2133–2136, ISSN 00948276, https://doi.org/10.1029/2000GL008479, 2000.

Steinhage, D., Kipfstuhl, S., Nixdorf, U., and Miller, H.: Internal structure of the ice sheet between Kohnen station and Dome Fuji, Antarctica, revealed by airborne radio-echo sounding, Annals of Glaciology, 54, 163–167, ISSN 02603055, https://doi.org/10.3189/2013AoG64A113, 2013.

Sutter, J., Fischer, H., Grosfeld, K., Karlsson, N. B., Kleiner, T., Van Liefferinge, B., and Eisen, O.: Modelling the Antarctic Ice Sheet across the mid-Pleistocene transition – Implications for Oldest Ice, The Cryosphere, 13, 2023–2041, ISSN 19940424, https://doi.org/10.5194/tc-13-2023-2019, 2019.

Sutter, J., Fischer, H., and Eisen, O.: Investigating the internal structure of the Antarctic ice sheet: The utility of isochrones for spatiotemporal ice-sheet model calibration, The Cryosphere, 15, 3839–3860, ISSN 19940424, https://doi.org/10.5194/tc-15-3839-2021, 2021.

The JAX authors: JAX: High-Performance Array Computing, 2024.

Van Liefferinge, B., Pattyn, F., Cavitte, M. G., Karlsson, N. B., Young, D. A., Sutter, J., and Eisen, O.: Promising oldest ice sites in East Antarctica based on thermodynamical modelling, The Cryosphere, 12, 2773–2787, ISSN 19940424, https://doi.org/10.5194/tc-12-2773-2018, 2018.

Vanderstraeten, A., Mattielli, N., Laruelle, G. G., Gili, S., Bory, A., Gabrielli, P., Boxho, S., Tison, J.-L., and Bonneville, S.: Identifying the provenance and quantifying the contribution of dust sources in EPICA Dronning Maud Land ice core (Antarctica) over the last deglaciation (7–27 kyr BP): A high-resolution, quantitative record from a new Rare Earth Element mixing model, Science of The Total Environment, 881, 163 450, ISSN 00489697, https://doi.org/10.1016/j.scitotenv.2023.163450, 2023.

Waddington, E. D., Neumann, T. A., Koutnik, M. R., Marshall, H.-P., and Morse, D. L.: Inference of accumulation-rate patterns from deep layers in glaciers and ice sheets, Journal of Glaciology, 53, 694–712, https://doi.org/10.3189/002214307784409351, 2007.

Wang, Z., Chung, A., Steinhage, D., Parrenin, F., Freitag, J., and Eisen, O.: Mapping age and basal conditions of ice in the Dome Fuji region, Antarctica, by combining radar internal layer stratigraphy and flow modeling, The Cryosphere, 17, 4297–4314, https://doi.org/10.5194/tc-17-4297-2023, 2023.

Watanabe, O., Jouzel, J., Johnsen, S., Parrenin, F., Shoji, H., and Yoshida, N.: Homogeneous climate variability across East Antarctica over the past three glacial cycles, Nature, 422, 509–512, ISSN 0028-0836, https://doi.org/10.1038/nature01525, 2003.

Wesche, C., Elsen, O., Oerter, H., Schulte, D., and Steinhage, D.: Surface topography and ice flow in the vicinity of the EDML deep-drilling site, Antarctica, Journal of Glaciology, 53, 442–448, ISSN 00221430, https://doi.org/10.3189/002214307783258512, 2007.

Westhoff, J., Ardoin, L., Weikusat, I., Blard, P. H., Fripiat, F., Seth, B., Soussaintjean, L., Krebs, M., Bouchet, M., Chung, A., Scoto, F., Lemburg, J., Lawer, G., Hüther, M., Stoll, N., Rathmann, N., Morici, L. C., Tison, J.-L., Eisen, O., Lilien, D., Mulvaney, R., Stocker, T., Koldtoft, I., Boeckmann, G., Hansen, S., Parrenin, F., Pattyn, F., Isaksson, E., Hansson, M., de Wal, R. v., Fischer, H., Landais, A., Barbante, C., Dahl-Jensen, D., and Wilhelms, F.: 316 m of ice beyond the stratified sections of the Beyond EPICA Little Dome C ice core, Nature Geoscience, https://doi.org/10.21203/rs.3.rs-9883712/v1, 2026.

Winter, A., Steinhage, D., Arnold, E. J., Blankenship, D. D., Cavitte, M. G. P., Corr, H. F. J., Paden, J. D., Urbini, S., Young, D. A., and Eisen, O.: Comparison of measurements from different radio-echo sounding systems and synchronization with the ice core at Dome C, Antarctica, The Cryosphere, 11, 653–668, ISSN 1994-0424, https://doi.org/10.5194/tc-11-653-2017, 2017.

Wolff, E., Brook, E. J., Dahl-Jensen, D., Fujii, Y., Jouzel, J., Lipenkov, V. Y., Severinghaus, J. P., Fischer, H., van Ommen, T., Bauska, T., and Higgins, J. A.: White paper: The oldest ice core: A 1.5 million year record of climate and greenhouse gases from Antarctica, International Partnerships in Ice Core Sciences, pp. 1–4, 2020.